Rubber-Modified Epoxies. III. Analysis of Experimental Trends through a Phase Separation Model

S. M. MOSCHIAR,[1] C. C. RICCARDI,[1] R. J. J. WILLIAMS,[1,*] D. VERCHERE,[2] H. SAUTEREAU,[2] and J. P. PASCAULT[2]

[1]Institute of Materials Science and Technology (INTEMA), University of Mar del Plata and National Research Council (CONICET), 7600 Mar del Plata, Argentina, and [2]Laboratoire des Matériaux Macromoléculaires, URA CNRS no. 507, Institut National des Sciences Appliquées de Lyon, 20, Avenue Albert Einstein, 69621 Villeurbanne Cedex, France

SYNOPSIS

A phase separation model was used to simulate the morphologies obtained in a system consisting of a diepoxide based on bisphenol-A diglycidylether cured with a cycloaliphatic diamine, in the presence of an epoxy-terminated butadiene-acrylonitrile random copolymer (ETBN). A detailed analysis of experimental factors affecting resulting morphologies was previously reported. The model, based on a thermodynamic description through a Flory–Huggins equation, and constitutive equations for polymerization and phase separation rates, could explain most of the observed trends. A nucleation-growth mechanism was believed to take place because of the very low values of interfacial tensions for this type of systems. Conditions which would lead to spinodal demixing are also discussed.

INTRODUCTION

In parts I and II of this series experimental results related to a phase separation process taking place in a particular rubber-modified epoxy were discussed.[1,2] A diepoxide based on bisphenol-A diglycidylether (DGEBA), was cured with a cycloaliphatic diamine (4,4′-diamino-3,3′-dimethyldicyclohexyl-methane, 3DCM), in the presence of an epoxy terminated butadiene–acrylonitrile random copolymer (ETBN). This last one was an adduct prepared by reacting the carboxyl groups of a CTBN (Hycar 1300 × 8, Goodrich) with an excess of DGEBA, in the presence of triphenylphosphine as catalyst.[1] Chemical structures of the different components of the formulation are shown in Figure 1.

In part I,[1] the influence of ETBN on the polymerization and phase separation processes was reported. In part II,[2] trends observed for the particle size distribution, the volume fraction of dispersed phase, the concentration of dispersed phase particles, and the composition of both phases as a function of polymerization temperature and rubber concentration were discussed. The aim of part III is to analyze the possibility of explaining the observed morphologies through a phase separation model previously reported.[3,4] Most of the necessary experimental information, i.e., polymerization kinetics, viscosity evolution, cloud-point conversions, is available.[1,5] The model will be applied to experimental runs carried out at 50°C and 75°C, and three different mass fractions of rubber, % R = 6.5, 10.6, and 15 (here and in what follows, "rubber" means the CTBN block of the ETBN triblock copolymer). Although experimental runs at 29°C and 100°C were also carried out,[2] their reliability for modeling purposes is not as good as the others due to the difficulty in matching temperature scales for runs at the lowest temperature, and time scales for runs at the highest temperature.

A global description of the phase separation process is shown in Figure 2. Initially ($p = 0$), the system is homogeneous; phase separation starts at the cloud-point conversion, p_{cp}, and the final morphology is arrested well before gelation (p_{gel}).[2]

The phase separation process will be described in terms of a nucleation-growth mechanism.[3,4] Its use derives from the fact that morphologies reported

* To whom correspondence should be addressed.

Journal of Applied Polymer Science, Vol. 42, 717–735 (1991)
 CCC 0021-8995/91/030717-19$04.00

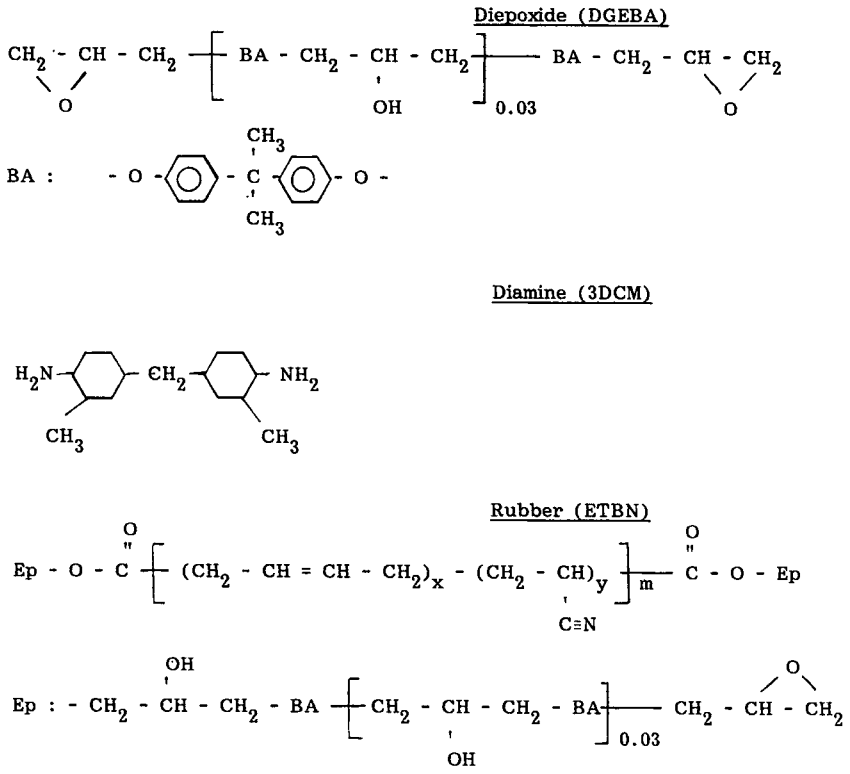

Figure 1 Chemical structures of diepoxide, diamine, and rubber.

in the literature usually consist of spherical domains dispersed in a continuous matrix. Most authors have used a nucleation-growth mechanism to describe these morphologies.[4,6–10] On the other hand, conditions under which spinodal decomposition may be the origin of the phase separation process have been discussed.[3] This kind of phase separation is usually assigned to textures displaying some degree of connectivity (most usually a co-continuous structure). Recently, Hsich[10] and Yamanaka et al.[11] gave experimental evidence of the presence of spinodal decomposition in fast reacting systems with compositions located close to the critical point (high rubber concentrations). Moreover, Yamanaka et al.[11] stated that the nucleation-growth mechanism is not expected to take place in any case mainly because of the fact that nucleation is recognized to be a very slow process. The spherical domain structure is schematically represented as arising from the evolution of an initial co-continuous structure, although no direct experimental evidence of this model could be obtained. This controversial statement will be discussed in relation to the experimental results obtained for our particular system.

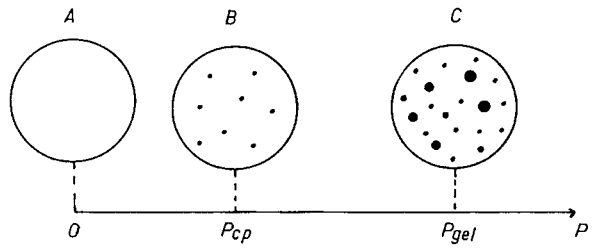

Figure 2 Stages during the phase separation process. (A) homogeneous solution for the unreacted system ($p = 0$); (B) beginning of phase separation at the cloud-point conversion (p_{cp}); (C) final morphology at p_{gel} (or at p_{vit} if vitrification takes place before gelation).

Table I shows morphological parameters obtained for samples containing different rubber amounts precured at 50°C and 75°C for periods long enough to go beyond gelation.[2] An increase in the initial rubber amount leads to an increase in the volume fraction of dispersed phase, the average diameter of particles and the rubber concentration remaining in the continuous phase after the arrest of phase separation. A temperature increase gives an increase in the size of particles while decreasing their concentration. The phase separation model has to provide an explanation for the ensemble of experimental results.

The model needs a thermodynamic analysis to predict the location of binodal and spinodal curves

Table I Morphological Parameters Obtained for Samples Containing Different Rubber Amounts Precured at 50°C for Enough Time to go Beyond Gelation[2]

ϕ_{Ro}	7.6		12.3		17.3	
% R	6.5		10.6		15	
T_i (°C)	50	75	50	75	50	75
$\bar{D}$ (SEM), μm	0.26	0.36	0.31	0.37	0.35	0.43
V_D (SEM)	0.107	0.089	0.132	0.172	0.254	0.248
P (SEM) × 10^{-12}	8.7	3.2	6.4	5.4	9.3	4.6
P (STEM) × 10^{-12} (part/cm^3)	3.8	2.2	5.7	2.8	5.0	2.6
ϕ_R^C (%)	2.9	3.1	4.1	4.3	6.4	6.1
$\overline{\phi_E^D}$ (%)	52.5	46.0	33.3	49.0	50.4	48.6

$\bar{D}$ (SEM) = number-average diameter of the population of dispersed phase particles derived from SEM micrographs; V_D (SEM) = volume fraction of dispersed phase derived from SEM micrographs; P (SEM) = number of particles of dispersed phase per unit volume, calculated from SEM micrographs; P (STEM) = number of particles of dispersed phase per unit volume, calculated from V_D (TEM) and the particle distribution derived from SEM; ϕ_R^C = volume fraction of rubber remaining in the matrix (continuous phase), at the end of phase separation; $\overline{\phi_E^D}$ = average volume fraction of epoxy–amine copolymer in dispersed phase domains (it is expressed as an average due to the possible phase segregation inside dispersed domains); ϕ_{Ro} = initial volume fraction of rubber in the formulation; % R = initial mass fraction of rubber in the formulation; T_i = precure temperature at which phase separation followed by gelation is produced.

SEM = scanning electron microscopy; TEM = transmission electron microscopy.

during polymerization, however, it also needs constitutive equations to express the phase separation and polymerization rates. Both aspects will be discussed further.

THERMODYNAMIC ANALYSIS

The initial system is regarded as a solution of two "components": the epoxy–amine copolymer, taken as a pure component, and the rubber, taken as the CTBN block of the ETBN triblock copolymer. Thus, a pseudobinary system is defined in such a way that component E (epoxy–amine) copolymer and component R (rubber), keep a constant overall volume fraction independently of the chemical bonds between the ETBN adduct and the epoxy–amine copolymer. Anyway, the concentration of epoxide equivalents in ETBN makes a very low fraction of the total epoxide amount, i.e., 2.4% for a formulation containing 15% R. Statistical calculations show that the average mass attached to ETBN becomes important only at higher conversions than the range at which most of the phase separation has taken place.

The free energy of mixing per unit volume is described by the Flory–Huggins equation:

$$\Delta G^V = (RT/\bar{V}_{Eo})[(\phi_E/Z_E)\mathrm{Ln}\ \phi_E + (\phi_R/Z_R)\mathrm{Ln}\ \phi_R + \chi\phi_E\phi_R] \quad (1)$$

where χ is the interaction parameter, ϕ_E and ϕ_R are the volume fractions of both components, and Z_E and Z_R are the ratios of molar volumes of both components with respect to the one taken as a reference,

$$Z_E = \bar{V}_E/\bar{V}_{Eo} \quad (2)$$

$$Z_R = \bar{V}_R/\bar{V}_{Eo} \quad (3)$$

V_{Eo} is the initial molar volume of the epoxy–amine copolymer, defined as

$$\bar{V}_{Eo} = \frac{(M_{A4} + 2M_{B2})}{3\rho_E} = 276.6\ \mathrm{cm^3\ mol^{-1}}$$

where M_{A4} and M_{B2} are the molecular weights of diamine and diepoxide, and ρ_E = 1.127 g cm^{-3}, is the density of the epoxy–amine copolymer.

While Z_R remains constant during polymerization (Z_R = 13.73), Z_E increases with the molecular weight,

$$Z_E = \bar{V}_E/\bar{V}_{Eo} = \overline{M_n}/\overline{M_{no}} \quad (4)$$

The number average molecular weight of the epoxy–amine copolymer may be calculated as

$$\overline{M_n} = \frac{\text{total mass}}{\text{total number of moles}} = \frac{A_4M_{A4} + B_2M_{B2}}{A_4 + B_2 - 4pA_4}$$

where the total number of moles is calculated as the initial number less the number of reacted diamine equivalents (each epoxy–amine bond decreases the number of molecules in one unit if there are no intramolecular cycles). But as the epoxy–amine formulation is stoichiometric, $B_2 = 2A_4$. Then,

$$Z_E = \overline{M_n}/\overline{M_{no}} = (1 - 4p/3)^{-1} \qquad (5)$$

It is interesting to regard that in eq. (1), the first two terms of the right-hand side represent the configurational entropy contribution to the free energy. The contribution of the first term is larger than the one of the second term due to the fact that $(\phi_E/Z_E) \gg (\phi_R/Z_R)$ for rubber-modified thermosets. Therefore, small changes in Z_E lead to high relative variations in the free energy of mixing. The increase of Z_E during polymerization is the main factor leading to phase separation.[3,4] For example, for a cloud-point conversion belonging to the experimental range,[2] $p_{cp} = 0.2$, $Z_E = 1.364$. Thus, a 36% increase in Z_E is enough to promote phase separation. In this regard, we have shown[12] that for unreactive epoxy–CTBN mixtures, the miscibility gap is highly dependent on the molecular mass of the epoxy prepolymer. Increasing $\overline{M_n}$ from 349 g mol^{-1} to 383, 479, and 550 g mol^{-1}, leads to an increase in the precipitation threshold temperature of some 14°C, 65°C, and 84°C, respectively. As this high increase is produced without changes in the calculated values of solubility parameters,[12] it may be concluded that it is the increase in the molecular weight of the epoxy–amine copolymer the origin of the phase separation process in rubber-modified epoxies.

Another factor to be discussed is the influence of the CTBN polydispersity on the thermodynamic analysis. In this regard, the location of the precipitation threshold at very low ϕ_R values revealed the effect of CTBN polydispersity.[12] Thermodynamic calculations of cloud-point curves taking the polydispersity of CTBN into account confirmed its influence on the location of the precipitation threshold.[13] However, it was also shown that a binodal curve considering monodisperse components could be used as a rough approximation to predict the composition of both phases in the course of a macroscopic phase separation.[12,13] This approximation is associated with the use of an apparent interaction parameter, χ, higher than the one resulting by considering the polydispersity of components.[13]

Starting from eq. (1), binodal curves in p vs. ϕ_R coordinates may be calculated using standard procedures,[3,4] once values of the interaction parameter are selected. Figure 3 shows several binodal curves

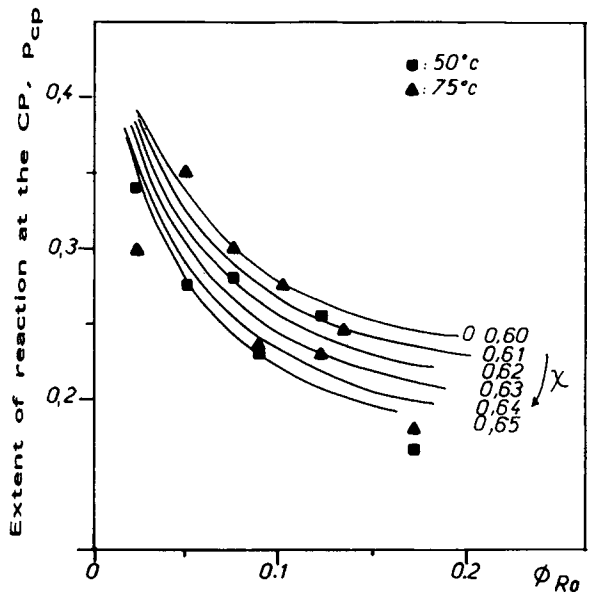

Figure 3 Binodal curves for different χ values in conversion vs. rubber volume fraction coordinates. Experimental points[1] of cloud-point conversions obtained at 50°C and 75°C are also shown.

in the range of χ values going from 0.60 to 0.65, together with experimental values of cloud-point conversions, p_{cp}, determined at 50°C and 75°C, for samples containing different initial rubber concentrations.[1] Due to the expected decrease in the interaction parameter with increasing temperatures, i.e., through a relationship of the type $\chi = A + B/T$, values at 50°C would have been observed below values at 75°C, for every rubber concentration. However, due to the range of experimental error in the p_{cp} determination, no trend among values obtained at both temperatures results are evident. Therefore, an average value of $\chi = 0.63$ will be used in the model for both temperatures. Later we will discuss the influence of introducing a χ vs. T relationship in model predictions.

It is interesting to compare the value of $\chi = 0.63$ with interaction parameters reported for unreactive epoxy–ETBN formulations,[12] i.e., systems devoid of diamine. In order to compare values on the same basis, it is convenient to express them per unit volume of system. Then, we define[12]

$$\Lambda = \chi RT/V_r,$$

where V_r is molar volume of the unit cell used to define χ. In our case, $V_r = \bar{V}_{Eo} = 276.6$ cm$^3 \cdot$ mol^{-1}. This leads to

$$\Lambda = 6.1 - 6.6 \text{ J/cm}^3 \text{ (in the 50–75°C range)}$$

This is exactly the same range of values reported[12] for the interaction parameter between an epoxy prepolymer and an ETBN (based on CTBNx8), at temperatures close to 300 K. Then, it may be stated that, for the particular system under study, the addition of the diamine does not introduce a significant variation on the value of the interaction parameter.

POLYMERIZATION RATE

Detailed studies of the kinetics of this epoxy–amine system, both with and without ETBN, were previously reported.[1,5] A unique kinetic expression could be obtained for systems containing different rubber amounts, as shown by Figure 4 for a polymerization carried out at 50°C.

Kinetics is expressed by the following constitutive equation[1,5]

$$dp/dt = K_1[0.0424 + p](1 - p) \times [0.75\alpha + 0.25\alpha^{0.2}] \quad (6)$$

$$p = 1 - 0.375\alpha - 0.625\alpha^{0.2}$$

$$K_1(\text{min}^{-1}) = 4.73.10^7 \exp(-6921/T)$$

where α is the ratio of primary amine hydrogens with respect to initial epoxy equivalents.

The expression takes into account the difference in reactivities of secondary and primary amines ($k_2/k_1 = 0.4$), and the presence of an initial ratio of hydroxyls with respect to epoxides equal to 0.0424. The full curve of Figure 4 represents the conversion vs. time relationship obtained from eq. (6) at 50°C.

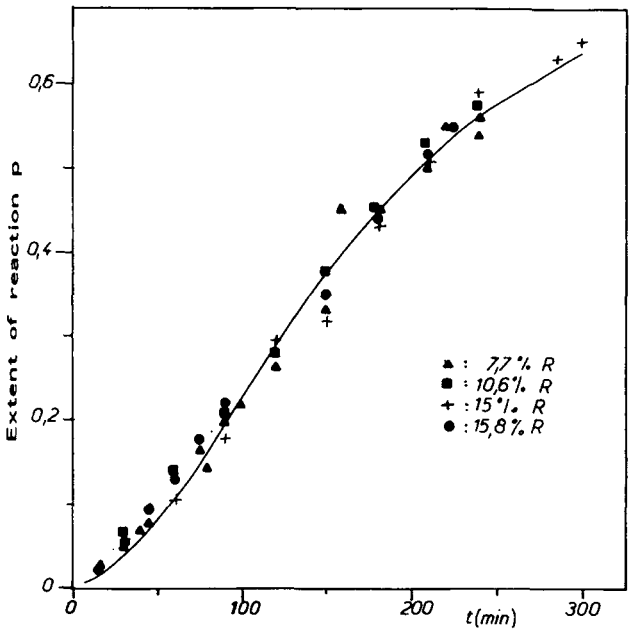

Figure 4 Conversion vs. time for samples containing different mass fractions of rubber (% R), polymerized at 50°C.

PHASE SEPARATION RATE

Nucleation Rate

Once the system enters the metastable region, the actual concentration of the rubber in the epoxy–amine copolymer (matrix), ϕ_R^C, is higher than the equilibrium value given by the binodal curve, ϕ_R^{eq}. Using methods previously described,[3,4] the instantaneous composition of the phase being segregated from the matrix, ϕ_R^D, and the free energy change per unit volume, ΔG_N, can be calculated. From this last value, the critical radius, r_c, and the free energy barrier at r_c, ΔG_N, can be determined.[3,4] They are given by

$$r_c = 2\sigma/|\Delta G_N| \quad (7)$$

$$\Delta G_c = 16\pi\sigma^3/3|\Delta G_N|^2 \quad (8)$$

where σ is the interfacial tension between both phases.

Let us consider the range of possible σ values. Sohn et al.[14] have recently reported interfacial tension values between α,ω methyl carboxylate–butadiene–acrylonitrile copolymers and an epoxy prepolymer, as a function of temperature and copolymer composition. For a CTBN having the same acrylonitrile fraction than the one used here, they reported a value of σ (55°C) = 0.58 mN/m (= dyn/cm), and a temperature dependence $d\sigma/dT = -(0.01 - 0.02)$ mN · m^{-1} °C^{-1}. However, it is well known[15,16] that a sharp decrease in interfacial tension is observed with the use of triblock copolymers like the ETBNs used in the present study. This arises mainly from the energetically preferred orientation of the blocks at the interface into their respective compatible phases. Moreover, in our case we are dealing with the segregation of a solution from a solution, both with different composition. Which is the interfacial tension in this case? Qualitatively, it may be assumed that it must have a very low value due to the possibility of orientation of similar components in both solutions. Thus, it is interesting to quote that a mass-fraction of CTBN of the order of 1% is enough to decrease the surface tension of a CTBN–epoxy solution to a value close to the one of pure CTBN.[17] Also, it was reported[18,19] that interfacial tensions of demixed polymer solutions derived from

polymer–polymer–solvent systems were in the range of 10^{-4}–10^{-1} mN/m.

For modeling purposes, we assume a law of the type

$$\sigma = \sigma_o(\phi_R^D - \phi_R^C) \tag{9}$$

which leads to $\sigma = 0$ when $\phi_R^D = \phi_R^C$, i.e., at the critical point. For the simulation we will take $\sigma_o = 0.05$ mN/m, although its variation in a broad range will be discussed.

The rate of homogeneous nucleation from condensed phases may be written as[20]

$$\frac{dP(r_c)}{dt} = N_o D_{AB} \exp(-\Delta G_c/kT) \tag{10}$$

where $P(r_c)$ is the volumetric concentration of particles with critical radius r_c (nuclei), N_o is an adjustable preexponential factor, D_{AB} is the diffusion coefficient of the rubber in the epoxy–amine copolymer and k is the Boltzmann constant.

The diffusion coefficient may be estimated from the Stokes–Einstein equation

$$D_{AB} = D_{AB}^o T/\eta(p, T) \tag{11}$$

where η is the viscosity of the solvent which, in our case, is taken as the viscosity of the epoxy–amine copolymer devoid of rubber. Thus, our estimation of D_{AB} constitutes an approximation valid in the limit of infinite dilution.

The initial viscosity, η_o, is given by[1]

$$\ln \eta_o(\text{Pa s}) = -14.09 + 4037/T(K) \tag{12}$$

Whereas the evolution of (η/η_o) with conversion may be expressed as a unique function of conversion from data previously reported,[1]

$$\ln(\eta/\eta_o) = 32.46p - 242.2p^2 + 1220p^3 - 2634p^4 + 2251p^5 \tag{13}$$

Equation (13) is represented on two different linear scales in Figure 5. The viscosity at the cloud point, η_{cp}, shows a high increase in the range of conversions where phase separation begins, i.e., from $p_{cp} = 0.15$ to 0.35 as results from Figure 3. Depending on the η_{cp} value for a particular formulation and polymerization temperature, different morphologies may be expected.[2,9]

A significant decrease in the value of the diffusion coefficient may be expected at conversions higher than $p = 0.4$ due to the high increase of viscosity in this range. This has been experimentally verified for a particular system.[6] An immediate consequence is the high drop in the nucleation rate which is expected in this range of conversions.

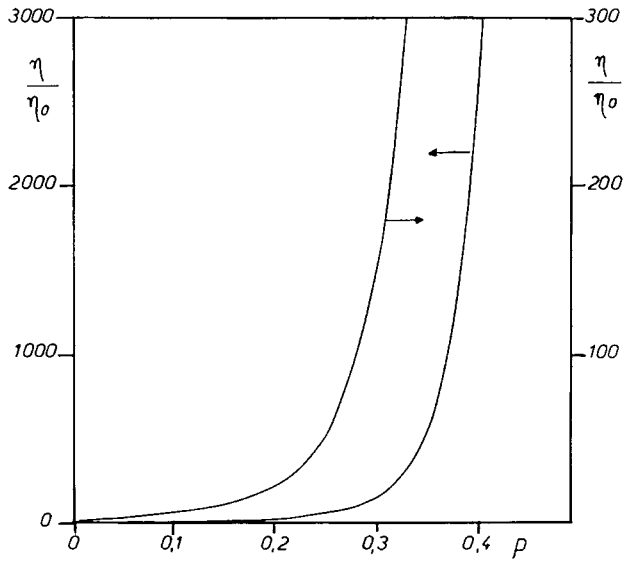

Figure 5 Increase of viscosity as a function of reaction extent depicted in two different scales.

In order to estimate the order of magnitude of D_{AB}^o, the empirical Wilke–Chang equation may be used[20,21]

$$D_{AB}^o = \frac{7.4.10^{-8}(\phi_S M_S)^{1/2}}{V_R^{0.6}} \quad [\text{cm}^2\,\text{s}^{-1}(\text{mPa s})\,\text{K}^{-1}] \tag{14}$$

where ϕ_S is an association factor for the solvent, M_S is the molecular weight of the solvent and V_R is the molar volume of rubber at its normal boiling point (expressed in $\text{cm}^3\,\text{mol}^{-1}$). Taking $\phi_S = 1$ and using initial values for M_S and V_R, it results

$$D_{AB}^o \cong 10^{-8}\,\text{cm}^2\,\text{s}^{-1}\,(\text{mPa S})\,\text{K}^{-1} \tag{15}$$

Considering that D_{AB}^o varies with composition and that eq. (14) is normally applied to low-molecular weight solutes at infinite dilution, eq. (15) must be regarded as an order-of-magnitude estimation. Actual values of D_{AB}^o used in the model were varied between 10^{-8} and $10^{-9}\,\text{cm}^2\,\text{s}^{-1}\,(\text{mPa s})\,\text{K}^{-1}$. Variations of ϕ_S, M_S, and V_R during conversion are outweighed by the variation of viscosity with extent of reaction.

A ratio between nucleation and polymerization rates may be defined as

$$N = dP(r_c)/dp \tag{16}$$

Growth Rate

As the system evolves in the metastable region particle growth takes place due to the driving force $(\phi_R^C - \phi_R^{eq})$, trying to restore the system to equilibrium. Let us define $dP(r')$ = number of particles per unit volume that were born at conversions between p' and $p' + dp$, and having an actual radius r' at the conversion p [when they were born, at $p = p'$, the radius was $r' = r_c(p')$].

The growth rate of every set of particles may be written as[4]

$$(4\pi/3)dP(r')dr'^3/dt = k_\phi 4\pi r'^2 dP(r')(\phi_R^C - \phi_R^{eq}) \tag{17}$$

Equation (17) gives the increase in volume fraction per unit time by the growth mechanism, through a proportionality with respect to the interfacial area per unit volume and the driving force. The proportionality coefficient is the mass transfer coefficient, k_ϕ. Its value is taken from the case of mass transfer from a stagnant medium to a sphere,[21]

$$k_\phi = D_{AB}/r' \tag{18}$$

Introducing eq. (18) into (17) and rearranging, we obtain

$$r'\frac{dr'}{dt} = D_{AB}(\phi_R^C - \phi_R^{eq}) \tag{19}$$

Thus, the growth rate is proportional to the product of the diffusion coefficient by the driving force. Similar to the nucleation rate, at $p = p_{gel}$, $D_{AB} \to 0$ and phase separation is arrested. However, well before gelation the growth rate will be negligible due to the very high viscosity value.

A ratio between growth and polymerization rates may be defined as

$$G = (r'dr')/dp \tag{20}$$

Coalescence Rate

The coalescence rate will be considered negligible due to the very high rate of viscosity increase.[3] In low-viscosity systems this mechanism may probably be present. An experimental evidence of this situation has been reported.[6]

STRUCTURE OF THE RUBBER-MODIFIED EPOXY

At any reaction extent p, the following calculations may be performed:

- Concentration of dispersed phase particles

$$P = \int_{p' \le p} dP(r') \tag{21}$$

- Cumulative distribution of particles with diameters lesser than or equal to an arbitrary value, D

$$P(D) = \int_{\substack{p' \le p \\ 2r' \le D}} dP(r') \tag{22}$$

- Size distribution function of dispersed phase particles

$$\frac{1}{P}\frac{dP(D)}{dD} \tag{23}$$

- Average diameter of dispersed phase particles

$$\bar{D} = \frac{1}{P}\int D\frac{dP(D)}{dD}\,dD \tag{24}$$

- Volume fraction of dispersed phase

$$V_D = (\pi/6)\int D^3\frac{dP(D)}{dD}\,dD \tag{25}$$

- Average composition of dispersed phase. The volume fraction $dV_D(p)$, demixed in the conversion range p and $p + dp$, has a composition ϕ_R^D, and may be calculated as

$$dV_D(p) = (4\pi/3)[r_c(p)]^3\,dP(r_c) + 4\pi\int_{p' \le p} r'^2\,dP(r')\,dr' \tag{26}$$

Then, the average volume fraction of rubber present in the dispersed phase is given by

$$\phi_R^D = \frac{1}{V_D}\int_{p' \le p} \phi_R^D(p')\,dV_D(p') \tag{27}$$

The average volume fraction of epoxy–amine copolymer in the dispersed phase results from

$$\overline{\phi_E^D} = 1 - \overline{\phi_R^D} \quad (28)$$

- Composition of the continuous phase

$$\phi_R^C = (\phi_{Ro} - V_D\overline{\phi_R^D})/(1 - V_D) \quad (29)$$

COMPARISON OF MODEL PREDICTIONS WITH EXPERIMENTAL RESULTS

Equations (10) and (19) were numerically solved using a Euler method, with the reaction extent p as the independent variable through eq. (6). Convergence was analyzed by varying the selected increment Δp.

Results shown in this section were obtained by fixing the following values for parameters appearing in the Flory–Huggins equation and the constitutive equations for phase separation: $\chi = 0.63$, $D_{AB}^{\circ} = 10^{-9}$ cm^2 s^{-1} (mPa s) K^{-1} and $\sigma_o = 0.05$ mN m^{-1}. The influence of their variation will be analyzed in the following section.

The value of the preexponential factor N_o [eq. (10)] was adjusted by comparing the experimental concentration of dispersed phase particles with model simulations. Figure 6 shows that a rough fitting of the six experimental runs results by taking $N_o = 2.10^{20}$ cm^{-5}. Independently of the particular N_o value, the model does predict an increase in the concentration of dispersed phase particles when decreasing the cure temperature. This results from the fact that the ratio $N_o = dP(r_c)/dp$ decreases when increasing temperature because the activation energy of polymerization (E/R = 6921 K) is higher than the one of nucleation (E_D/R = 4037 K, as results from eqs. (10)–(12)). This means that polymerization rate increases faster with temperature than nucleation rate.

Figure 7 shows a conversion vs. rubber concentration phase diagram with the location of binodal and spinodal curves. When the system enters the metastable region located between both curves, phase separation by the nucleation-growth mechanism begins to take place. The trajectory of the matrix composition, ϕ_R^C, depends on the relative rates of phase separation and polymerization. If the former is very much higher than the latter, the trajectory will approach the binodal and so will do the trajectory of the instantaneous composition of the phase demixed from the matrix, ϕ_R^D. If, on the other hand, the polymerization rate is very much higher

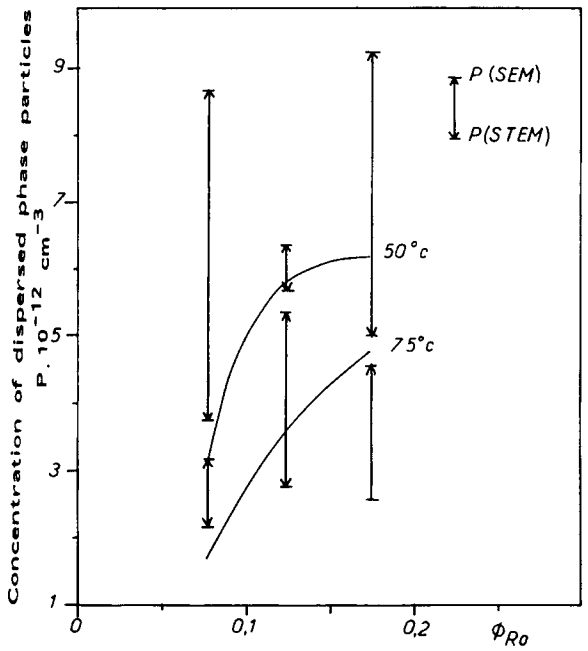

Figure 6 Comparison of experimental concentration of dispersed phase particles obtained by SEM and STEM measurements,[2] with model simulations for $N_o = 2.10^{20}$ cm^{-5}. Runs correspond to two different temperatures and three different initial rubber concentrations.

than the phase separation rate, an almost vertical trajectory for ϕ_R^C will be obtained and spinodal decomposition will take place. The simulation shown in Figure 7 represents an intermediate case.

An interesting observation is the fact that ϕ_R^C does not practically change beyond $p = 0.4$. This was expected from the high viscosity increase in this conversion range (Fig. 5). Therefore, most of the phase separation takes place at conversions close to the cloud-point. For the same reason, the average rubber concentration in dispersed domains, $\overline{\phi_R^D}$, has a value which is representative of the first stages of phase separation. Although, the phase demixed at high conversions is very rich in rubber, it makes a small contribution to the volume fraction of dispersed phase present in the system.

Regarding the location of the average composition of dispersed domains in the conversion vs. composition diagram, Figure 7 shows that it lies in the unstable region, i.e., inside the spinodal, at the end of phase separation. Therefore, it may be stated that phase separation must take place inside dispersed domains during polymerization. If this phase separation process drives the system to equilibrium, the average composition of separated phases inside dispersed domains must be read at the intersections of

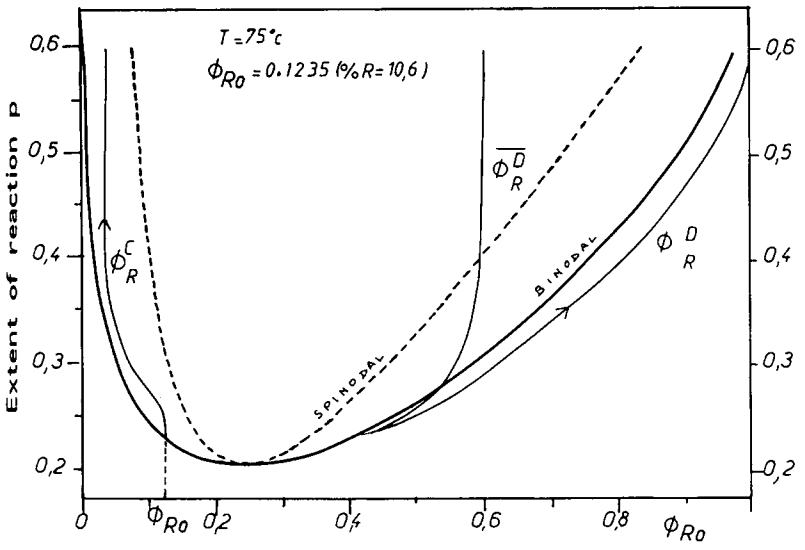

Figure 7 Conversion vs. rubber concentration phase diagram, showing binodal and spinodal curves and the evolution of the rubber concentration in the continuous phase, ϕ_R^C, and the dispersed phase (ϕ_R^D: instantaneous value, $\overline{\phi_R^D}$: average value), for a simulation at T = 75°C and % R = 10.6.

the horizontal line at p = 0.6 and the binodal. We see that compositions are very close to pure rubber and pure epoxy–amine copolymer. This is precisely what was inferred from the relaxations observed using dynamic mechanical measurements.[2] Then, the simulation gives an overall idea of the composition changes in the different phases present in the system.

Figure 8 shows a comparison of trajectories in the metastable region for polymerizations carried out at different temperatures, starting from different initial rubber concentrations. The polymerization carried out at 50°C (% R = 10.6) gives more phase separation than the one at 75°C (% R = 10.6), i.e., less ϕ_R^C starting from the same ϕ_{Ro}, because of the increase in the ratio of phase separation rate with respect to polymerization rate when decreasing temperature (E_D/R is the same for nucleation and growth rates). On the other hand, polymerizations starting from greater values of ϕ_{Ro} (75°C) show much more phase separation than those that start at lower values, at the same temperature. This is due to the decrease in both the cloud-point conversion and the associated viscosity when increasing the initial rubber concentration. This, in turn, increases the phase separation rate at a constant temperature. It is evident that the viscosity at the cloud point, η_{cp}, is a very significant parameter in the phase separation process. However, when compared with experimental results, we see that the simulation overestimates the amount of separated phase at % R = 15 while it underestimates the corresponding amount at % R = 6.5, as is shown in Figure 9. Although the predicted trend is correct in V_D vs. ϕ_{Ro} coordinates, it is not so in ϕ_R^C vs. ϕ_{Ro} coordinates (the crossover of curves shown in Figure 8 does not correspond to experimental values showing an increase of ϕ_R^C with ϕ_{Ro}).

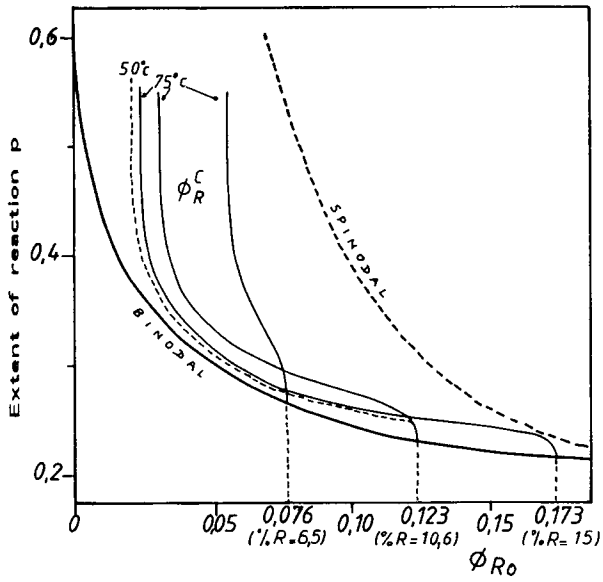

Figure 8 Comparison of trajectories in the metastable region for polymerizations carried out at different temperatures starting from different initial rubber concentrations.

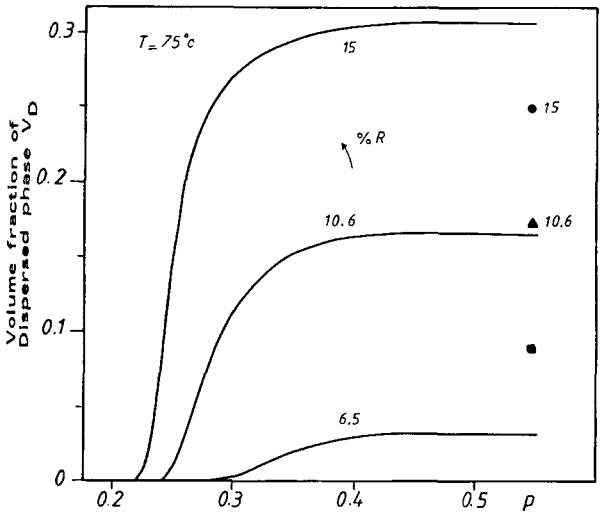

Figure 9 Volume fraction of dispersed phase as a function of reaction extent for polymerizations carried out at 75°C starting from different initial rubber concentrations. Points represent experimental values while full curves are model simulations.

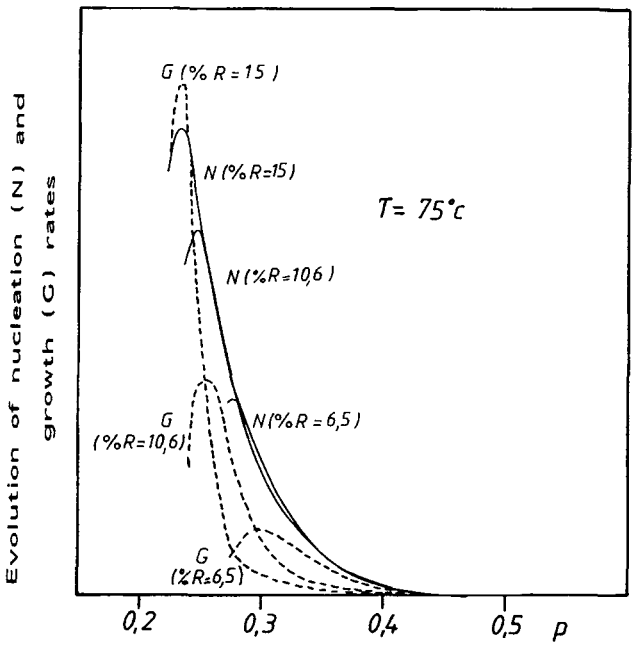

Figure 11 Evolution of nucleation (N), and growth rates (G) with respect to polymerization rate, as a function of conversion, in arbitrary scales.

Figure 10 represents the evolution of the average diameter of dispersed phase particles as a function of conversion for samples containing different initial rubber concentrations. Both the increase in the size of dispersed phase particles with ϕ_{Ro} as well as the low parametric sensitivity are predicted by the model. This last result arises from the counterbalance between the factors D_{AB} and $(\phi_R^G - \phi_R^{eq})$ appearing in the constitutive equation for the growth rate [eq. (19)]. This effect is evident in Figure 11, where the evolution of nucleation (N) and growth rates (G), with respect to polymerization rate [eqs. (16) and (20)], are depicted as a function of extent

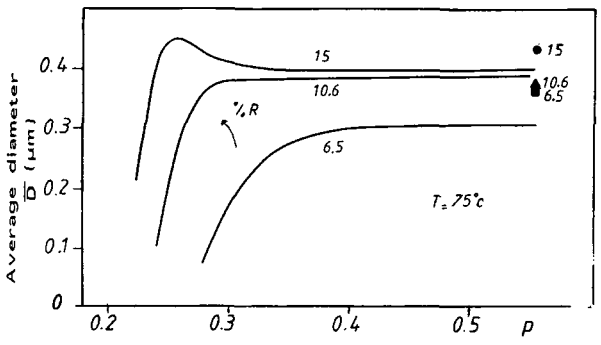

Figure 10 Average diameter of dispersed phase particles as a function of reaction extent for polymerizations carried out at 75°C starting from different initial rubber concentrations. Points represent experimental values while full curves are model simulations.

of reaction. Although the sample containing 15% R shows large initial values of both N and G, the latter decreases sharply with conversion due to the approach of the trajectory to the binodal curve and the resulting decrease in the driving force. Oppositely, the sample with 6.5% R shows a low initial growth rate due to the lower value of D_{AB} (higher viscosity). However, the high driving force keeps the low G value at a significant level in a broad conversion range (there is a crossover of G curves). This is the reason why the size of domains resulting for the sample containing 15% R are close to the ones obtained using 10.6% and 6.5% R. It is interesting also to note the decrease in $\bar{D}$ with p observed in Figure 10 for an intermediate range of conversion values. This is the consequence of the sharp decrease in the growth rate at these conversions, making sure that particles born in this range do not attain large sizes. This produces a decrease in the average size of the whole population and leads to a bimodal distribution of diameters, as will be discussed later.

Figures 12 and 13 represent the same trends as Figures 9 and 10, for samples polymerized at 50°C. We have reported in a previous part of the series[2] that SEM micrographs of samples containing 15% R and cured at 50°C, showed practically no differences beyond the first conversion where measurements could be performed (p close to 0.44). It may

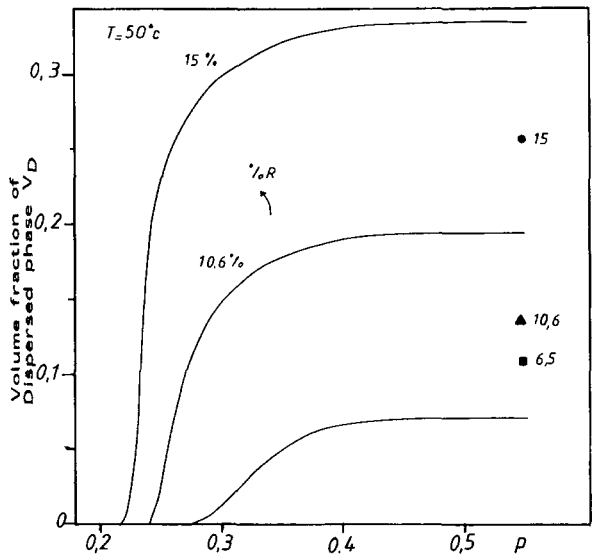

Figure 12 Volume fraction of dispersed phase as a function of reaction extent for polymerizations carried out at 50°C starting from different initial rubber concentrations. Points represent experimental values while full curves are model simulations.

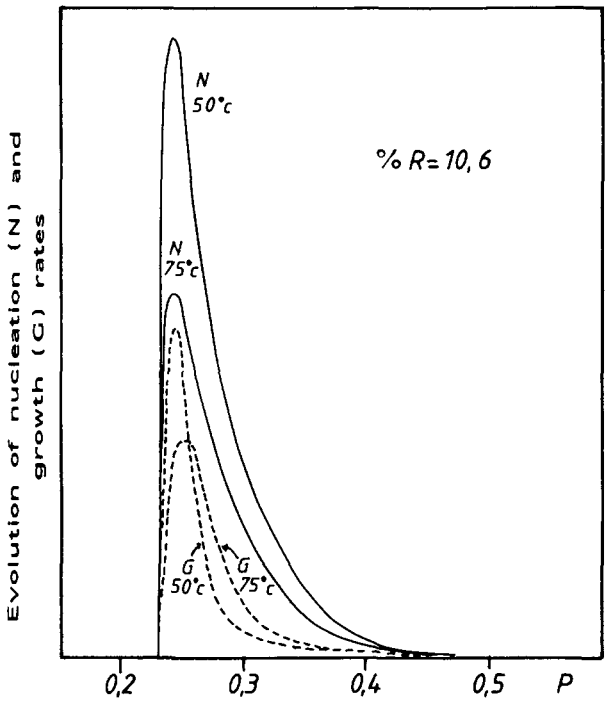

Figure 14 Evolution of nucleation (N) and growth rates (G) with respect to polymerization rate, as a function of conversion in arbitrary units.

be seen that the simulation agrees with this experimental finding well before $p = 0.44$. As it was already discussed, this arises from the fact that most of the phase separation takes place in a narrow range of conversions close to the cloud point.

In order to discuss more closely the effect of polymerization temperature on morphology, Figure 14 shows the ratios of nucleation (N) and growth (G) rates, with respect to polymerization rate, as a function of conversion at 50°C and 75°C. Both N and G are initially higher at 50°C than at 75°C, as previously explained. However G at 75°C keeps a significant value in a broader conversion range than G at 50°C (a crossover of curves is observed). This is due to the higher driving force at 75°C than at 50°C. The consequence is observed in Figure 15 where the simulation correctly predicts a larger average size at 75°C than at 50°C.

The model does always predict a higher V_D the lower the temperature. Differences in V_D values at 50°C and 75°C are slight as may be seen in Figure 16. However, for this particular rubber concentration experimental values are inversed (Table I and Fig.

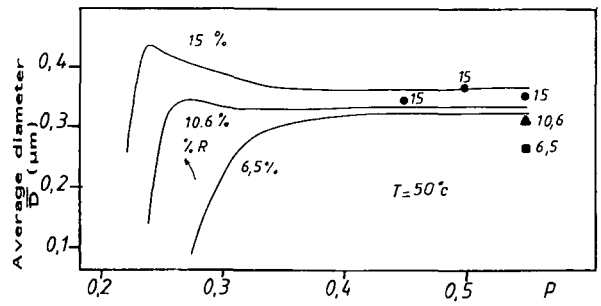

Figure 13 Average diameter of dispersed phase particles as a function of reaction extent for polymerizations carried out at 50°C starting from different initial rubber concentrations. Points represent experimental values while full curves are model simulations.

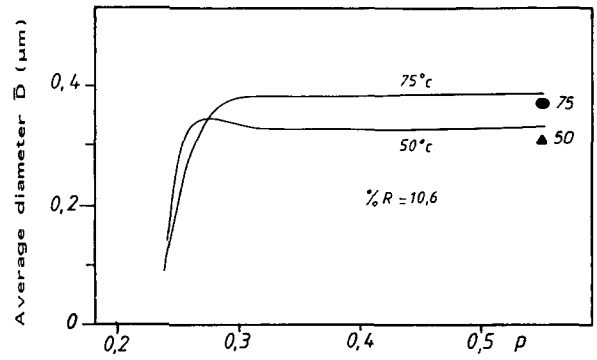

Figure 15 Average diameter of dispersed phase particles as a function of reaction extent for samples containing 10.6% R, polymerized at 50°C and 75°C. Points represent experimental values while full curves are model simulations.

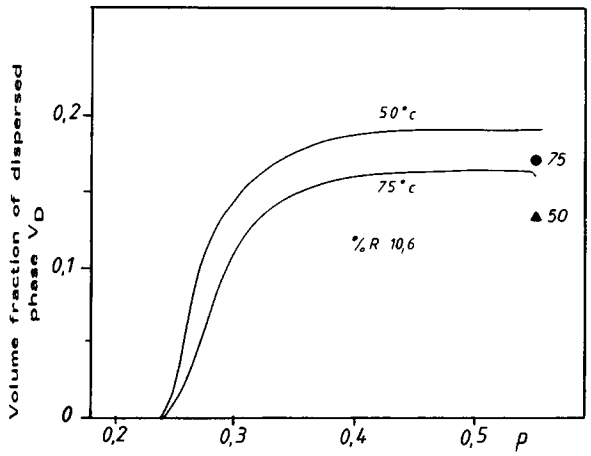

Figure 16 Volume fraction of dispersed phase as a function of reaction extent for samples containing 10.6% R, polymerized at 50°C and 75°C. Points represent experimental values while full curves are model simulations.

16). Anyway, the small variation of V_D with polymerization temperature which was experimentally observed, is indeed predicted by the simulation.

Figure 17 shows a comparison between experimental and predicted values for the compositions of both phases. As discussed in a previous part of the series,[2] reported experimental compositions were, in fact, calculated from direct observations, assuming the validity of Fox equation (for ϕ_R^C) and also the reliability of V_D (SEM) values (for $\overline{\phi_E^D}$). This implies that points should be more correctly represented by bars. In this sense, it may be stated that the simulation gives a rough prediction of the compositions of both phases. However, as previously discussed, the trend representing the variation of ϕ_R^C with ϕ_{Ro} is incorrectly predicted.

Figure 18 [(a)–(f)] shows a comparison between experimental and predicted particle size distributions. Overall, the simulation gives a reasonable prediction of the observed range of particle sizes, but does not fit the shape of the actual particle size distribution. The predicted shape depends on polymerization conditions. For % R = 6.5 [Fig. 18 (a and b)], the maximum of the predicted distribution is located at the largest sizes because of the significant growth rate in the conversion range where particles are born. Thus, in turn, is a consequence of the significant value of the driving force ($\phi_R^C - \phi_R^{eq}$). For % R = 10.6 and 15 [Fig. 18 (c to f)] bimodal distributions are predicted. The relative importance of the peak of small particles increases with the rubber amount and with a decrease in temperature. Under these conditions the trajectory in the metastable region evolves rapidly toward the binodal leading to a sharp decrease of the driving force for growing. Therefore, the large fraction of particles born in these conditions will only attain small sizes. Although it is very difficult to interpret experimental results in terms of unimodal or bimodal distributions, due to the very narrow range of particle sizes, it is suggestive to find an aspect of a bimodal distribution at low temperatures and high % R conditions [Fig. 18 (c, e, and f)].

INFLUENCE OF DIFFERENT PARAMETERS ON THE PHASE SEPARATION PROCESS

In the previous section a comparison of model predictions with experimental results was provided by taking $\chi = 0.63$, $D_{AB}^{\circ} = 10^{-9}$ cm^2 s^{-1} (mPa s) K^{-1} and, $\sigma_o = 0.05$ mN m^{-1}. In this section the effect of varying these parameters will be shown.

Influence of χ

Rubber-modified epoxies show an UCST (upper critical solution temperature) behavior.[12] Thus, a dependence of χ on temperature of the type $\chi = A + B/T$, with $B > 0$, is commonly used to account for this fact.[3,4] In our case, the $\chi(T)$ relationship was masked by the range of uncertainty in experimental results (Fig. 3). A single value of $\chi = 0.63$ was taken for the simulation, although the range

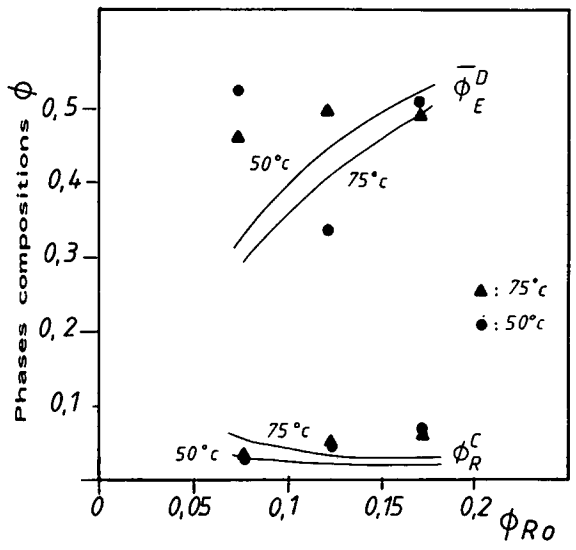

Figure 17 Average composition of epoxy–amine copolymer in dispersed domains, $\overline{\phi_E^D}$, and rubber volume fraction remaining in the matrix, ϕ_R^C, as a function of the initial rubber concentration, ϕ_{Ro}. Points represent experimental values while full curves are model simulations.

representing most of the experimental points lies between 0.60 and 0.65 (Fig. 3). The effect of varying χ in this range will be now discussed.

Figure 19 shows the location of binodals and trajectories in the metastable region for several χ values, represented in a conversion vs. rubber volume fraction phase diagram. The higher the χ value (low temperatures), the smaller the conversion and associated viscosity at the beginning of phase separation. This leads to an increase in the volume fraction of dispersed phase as is shown in Figure 20. However, for $\chi = 0.61$ the trajectory in the metastable region is the one associated with the highest driving force ($\phi_R^C - \phi_R^{eq}$) for the growth of particles. The consequence is that the more miscible system, i.e., the one polymerized at the highest temperature (simulated by $\chi = 0.61$) shows the least number of particles per unit volume but the greatest average diameter (Fig. 21). This may also explain the increase in the average size of dispersed phase domains which was experimentally observed when increasing the polymerization temperature.[2]

The situation is no longer the same when large variations of the interaction parameter χ are produced by changing the type of rubber, i.e., the fraction of acrylonitrile (AN) content. For example, a CTBN×13 (26% AN) is much more miscible with an epoxy prepolymer than a CTBN×8 (18% AN),[12] and the same is valid for the corresponding ETBN adducts. By using ETBN(×13) instead of ETBN(×8) one would expect to produce the phase separation at higher conversions (in the limit of $p_{cp} > 0.6$ no phase separation will take place at all before gelation). The relatively high viscosities at the cloud point will prevent the growth of particles to a large size. Thus, one would expect to have a decrease in both the volume fraction of dispersed phase (a general trend when decreasing χ) and in the average diameter (in Fig. 21 the average diameter at the end of phase separation goes through a maximum when decreasing χ below 0.60). Experimental results for our particular system, showed that the use of ETBN×13 (instead of ETBN×8), at a 15% R concentration and 75°C), lead to $p_{cp} \cong 0.3$–0.35 and $\bar{D} = 0.18$ μm (instead of 0.43 μm for ETBN×8). Also, for a particular DGEBA–polyoxypropylene amine system, it was reported that $\bar{D}$ decreased from 2 μm to 0.5 μm when using CTBN×13 instead of CTBN×8.[10]

Influence of D_{AB}

Figure 22 shows the effect of varying the selected D_{AB}^o value in ±50%, on the location of trajectories in the metastable region. The higher D_{AB}^o the greater the amount of phase separation, as shown in Figure 23. For the lowest D_{AB}^o value the spinodal is reached during the evolution of the system in the pregel stage. Again, the trajectory that is more apart from the binodal (highest driving force for the growth of particles), leads to the least number of particles per unit volume but the greatest average diameter (Fig. 24).

It is interesting to analyze the influence of a change in the viscosity of the system, without modifying any other parameter as T, D_{AB}^o or % R. Then, increasing viscosity leads to a decrease in the diffusion coefficient D_{AB} which, in turn, produces an increase in the average size of dispersed phase particles (Fig. 24). This is just the opposite trend as the one arising from ln η_{cp} vs. $\bar{D}$ reported in a previous part of the series.[2] The negative slope of this empirical relationship showed that the lower the viscosity at the cloud point the greater the average diameter. However, what was in fact changed to obtain experimental curves was either the polymerization temperature or the initial rubber concentration. But, when analyzing the influence of varying temperature or % R on the phase separation process, the observed experimental trends could be explained. This shows us that it is not possible to reduce the explanation of resulting morphologies to the value of a key parameter as the viscosity at the cloud point, but modifications introduced in the thermodynamic compatibility and rate of phase separation have to be analyzed together through a phase separation model as the one described here.

An experimental possibility of modifying the D_{AB}^o value without significantly changing the thermodynamics of the system is to use an ETBN based on a CTBN×8 but with a higher molecular mass than the usual commercial product. Increasing the number average molecular weight of the rubber from 3600 to 6900 led to a similar conversion at the cloud point but to a $\bar{D} = 0.62$ μm instead of 0.35 μm, for samples polymerized at 50°C.[17] The volume fraction of dispersed phase was reduced from 0.254 to 0.231 when using the larger mass. These trends may be explained by the increase in V_R [eq. (14)] and the corresponding decrease in D_{AB}^o.

Influence of σ_o

Figure 25 shows the effect of varying the selected σ_o value on the location of trajectories in the metastable region. It is seen that for $\sigma_o \leqq 0.01$ mN m^{-1} all the trajectories are equivalent, i.e., there is no effect of the value of σ_o on the phase separation process. This

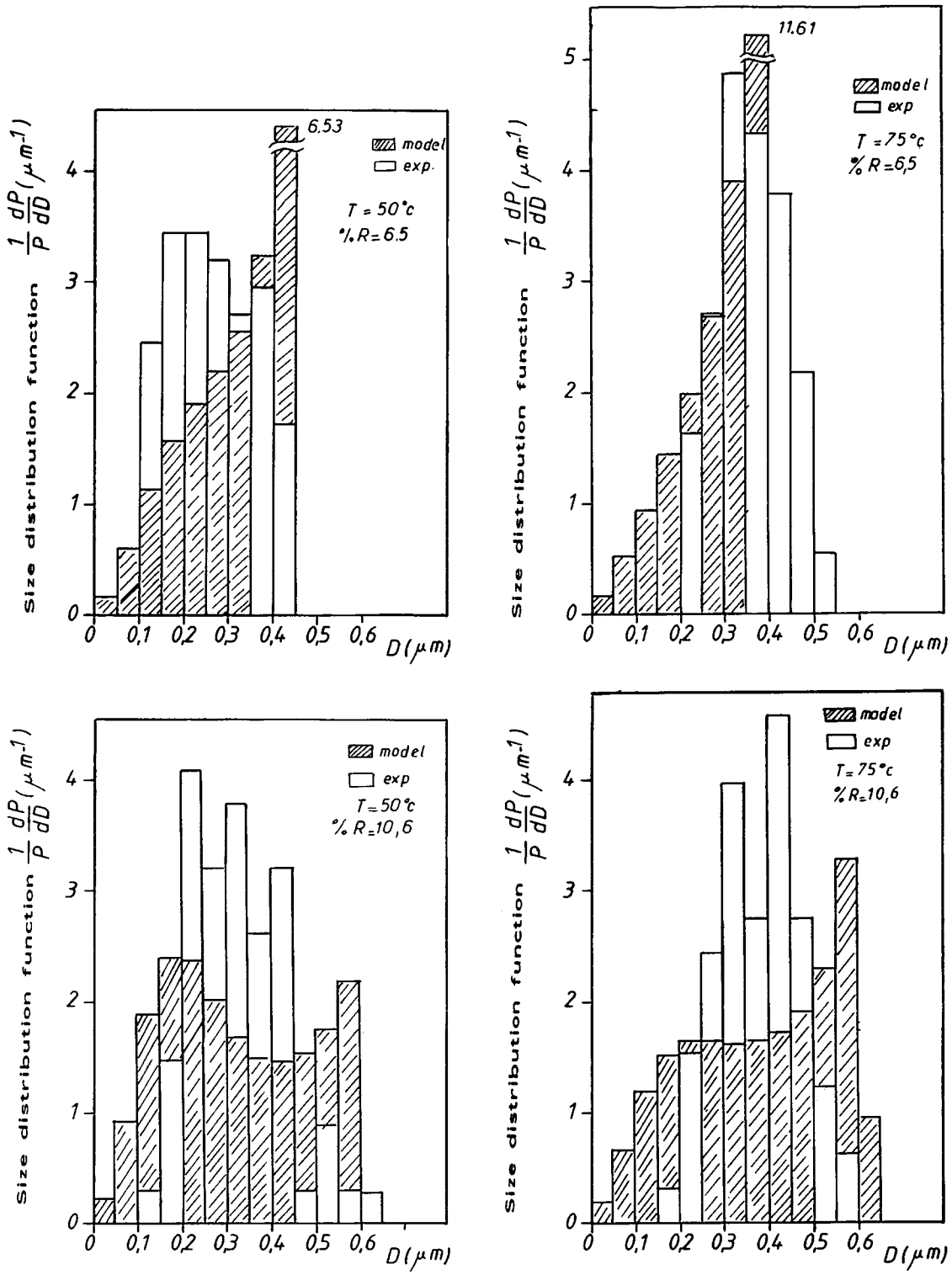

Figure 18 Comparison of particle size distributions for different polymerization conditions (the larger fraction is depicted behind the smaller one). (a) 50°C, % R = 6.5; (b) 75°C, % R = 6.5; (c) 50°C, % R = 10.6; (d) 75°C, % R = 10.6; (e) 50°C, % R = 15; (f) 75°C, % R = 15.

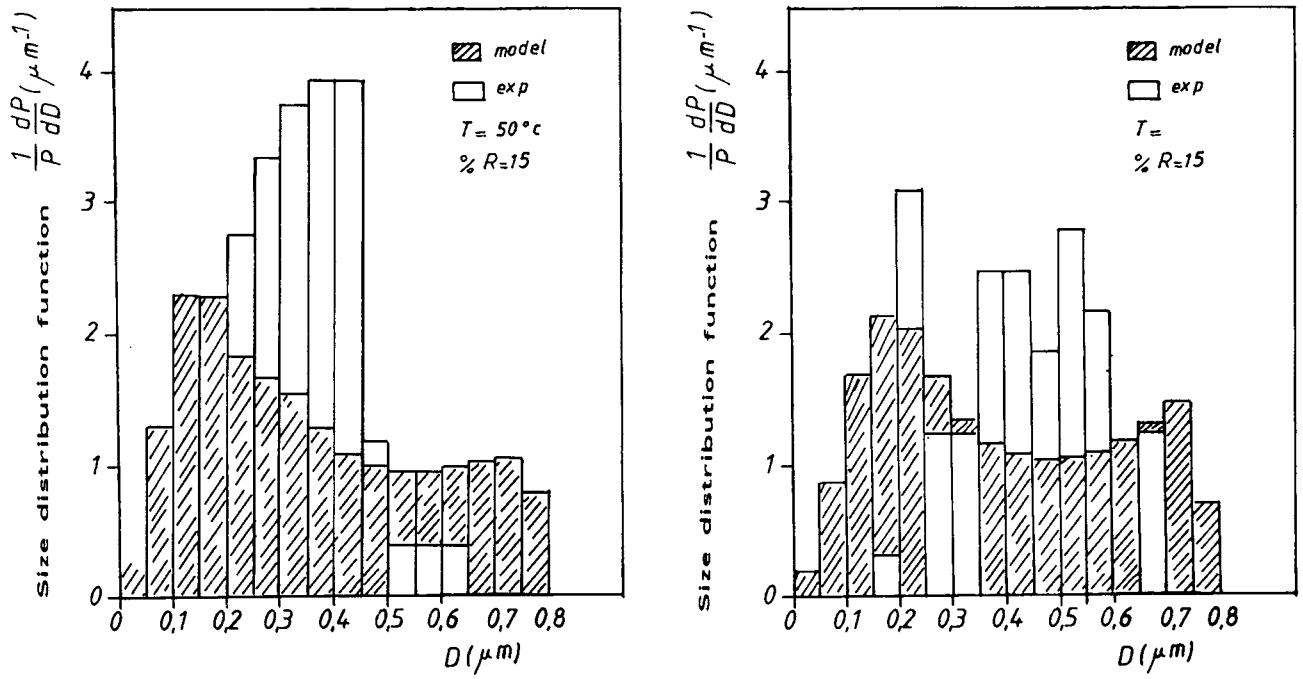

Figure 18 (*Continued from the previous page.*)

was the conclusion that we had previously reported.[3,4] However, these simulations were performed using values of σ_o in the range where no influence is actually observed (even if stated values of σ_o were higher, as was correctly shown by Sohn et al.[14]). We now see that if σ_o is allowed to increase beyond 0.1 mN m^{-1} spinodal decomposition is rapidly attained. For σ_o = 0.4 mN m^{-1} there is practically no phase separation by the nucleation-growth mechanism and demixing proceeds by spinodal decomposition. The value of σ_o = 0.05 mN m^{-1} used in the simulation is very close to the limit where no influence is observed. Therefore, the value of the interfacial tension is indeed very significant to establish the mechanisms of phase separation.

For the case of polymer blends (mixtures of un-

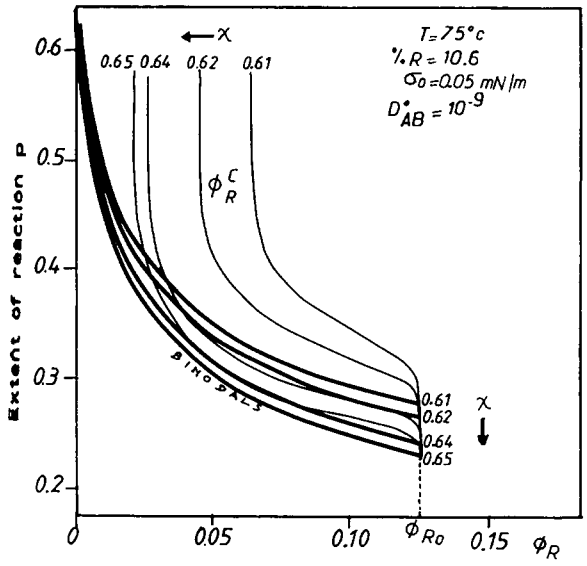

Figure 19 Conversion vs. rubber volume fraction phase diagram showing the location of binodals and trajectories in the metastable region for several values.

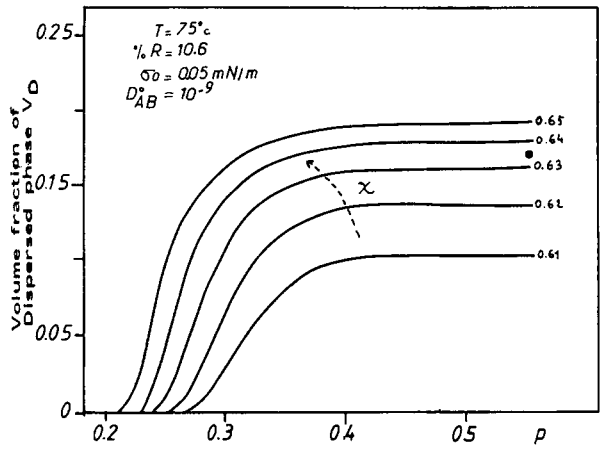

Figure 20 Volume fraction of dispersed phase as a function of reaction extent for different values of the interaction parameter, χ. The point represents the experimental value obtained under the specified polymerization conditions.

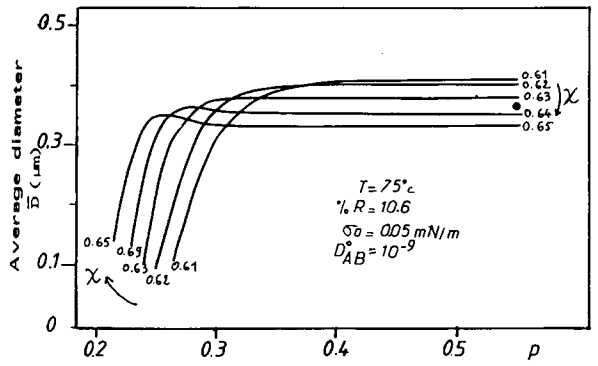

Figure 21 Average diameter of dispersed phase particles as a function of reaction extent for different values of the interaction parameter, χ. The point represents the experimental value obtained under the specified polymerization conditions.

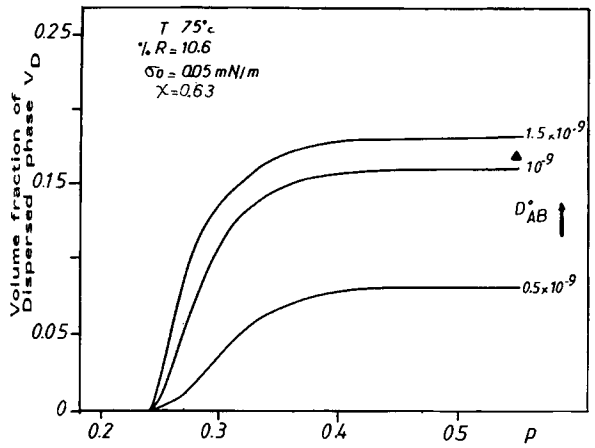

Figure 23 Volume fraction of dispersed phase as a function of reaction extent for different values of the diffusion coefficient, D°_{AB}. The point represents the experimental value obtained under the specified polymerization conditions.

reactive, high molecular weight thermoplastics), reported values of the interfacial tension[22] lie in the range 0.5–11 mN m^{-1}. This is the reason why spinodal decomposition is the frequent mechanism observed for phase separation in these systems. However, the extrapolation to polymer–polymer–solvent systems or to the demixing of solutions with a relative small change in composition (as in the present case), is not correct due to the very low values of the interfacial tensions in these cases. In rubber-modified epoxies the nucleation-growth mechanism is responsible for the phase separation process in most of the reported results. The possibility of spinodal demixing is, however, to be taken into account for fast polymerizing systems and/or for compositions located close to the critical point (in our particular system, results of the simulation for a sample containing 20% R led always to spinodal decomposition. This may explain the different trends for this particular sample reported previously[2]). It is precisely under these conditions (i.e., fast reactive systems and compositions close to the critical point) that spinodal decomposition has been obtained.[10,11]

The influence of the σ_o value on resulting morphologies is shown in Figures 26 and 27. Increasing σ_o (always in the range where phase separation proceeds by nucleation-growth) leads to a decrease in

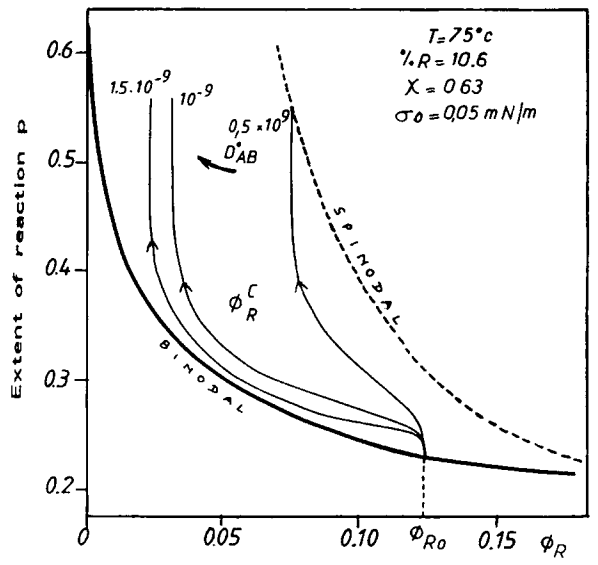

Figure 22 Conversion vs. rubber volume fraction phase diagram showing the location of binodal and spinodal curves, and trajectories in the metastable region for different values of the diffusion coefficient.

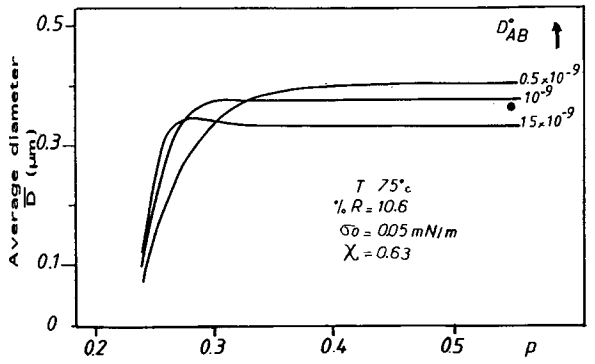

Figure 24 Average diameter of dispersed phase particles as a function of reaction extent for different values of the diffusion coefficient, D°_{AB}. The point represents the experimental value obtained under the specified polymerization conditions.

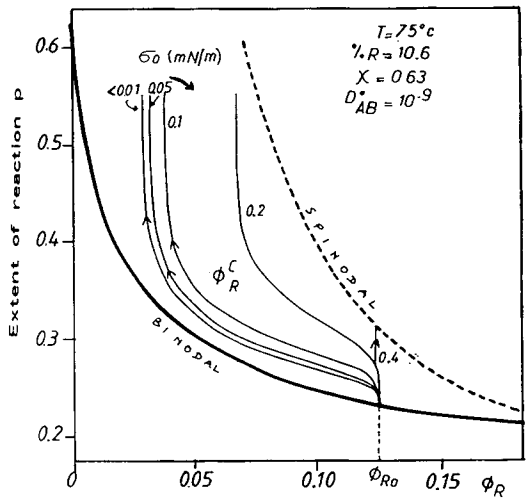

Figure 25 Conversion vs. rubber volume fraction phase diagram showing the location of binodal and spinodal curves together with trajectories in the metastable region for different values of the interfacial tension.

the volume fraction of dispersed phase, a decrease in the concentration of particles per unit volume, and an increase in the average size of the populations. The explanation is the same as that given for the influence of χ and D°_{AB}.

CONCLUSIONS

The phase separation model previously reported[3,4] was applied to a particular system where a detailed analysis of polymerization kinetics,[5] influence of the

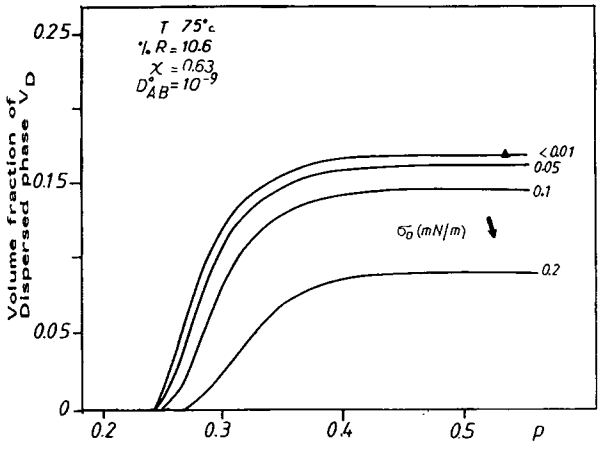

Figure 26 Volume fraction of dispersed phase as a function of reaction extent for different values of the interfacial tension, σ_o. The point represents the experimental value obtained under the specified polymerization conditions.

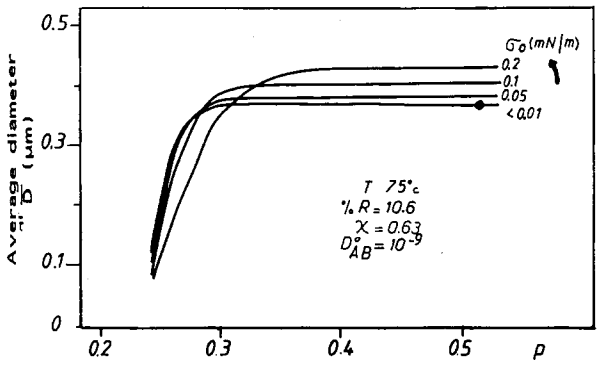

Figure 27 Average diameter of dispersed phase particles as a function of reaction extent for different values of the interfacial tension, σ_o. The point represents the experimental value obtained under the specified polymerization conditions.

rubber on kinetics, viscosity evolution and phase separation process,[1] and influence of polymerization temperature and rubber concentration on resulting morphologies,[2] was available. This constituted a severe examination of the proposed model.

Results discussed in the previous sections lead to the conclusion that the model can explain most of the observed trends on a qualitative rather than in a truly quantitative basis. This arises from the approximations and hypotheses used to describe the system, i.e., the thermodynamic description in terms of monodisperse components, the use of an interaction parameter independent of composition, and the rather simple laws used to describe nucleation and growth (i.e., use of viscosity at infinite dilution, use of the mass transfer coefficient for an isolated sphere in a stagnant medium).

The following experimental trends were correctly predicted and explained by the phase separation model:

(a) The volume fraction of dispersed phase (V_D) and the average size ($\bar{D}$) both increase with % R because phase separation takes place at lower conversions and corresponding lower viscosities. The influence on V_D is much more significant than on $\bar{D}$ because of the opposite effect of the increase of the driving force for growth when decreasing % R.

(b) The average size of particles, $\bar{D}$, increases with polymerization temperature because of two effects: (i) the increase in the driving force for growth due to the increase in the polymerization rate with respect to the phase separation rate ($E > E_D$); (ii) the decrease in the interaction parameter, χ, giving an ex-

tra increase of the driving force for growth (but decreasing the amount of phase separation). It is important to realize, however, that for a large temperature increase the situation may be different. For example χ may be so low that the system remains completely miscible (no phase separation at all), or, if demixed, particles do not attain large sizes due to the high viscosities (arising from the high conversion levels), and/or to the narrow conversion range where phase separation is allowed to proceed. Therefore, the functionality of $\bar{D}$ vs. T must show a maximum as has been experimentally found[7,23] and theoretically predicted.[3]

(c) The volume fraction of dispersed phase, V_D, decreases with polymerization temperature but does not show a very significant variation. This is due to the fact that the increase in both the diffusion coefficient and the miscibility (decrease of χ), are somewhat counterbalanced. However, a large temperature increase leads to a high decrease in V_D for reasons discussed in (b). This has been also experimentally found.[7,8]

(d) The average size of dispersed phase particles, $\bar{D}$, is arrested well before gelation due to the high increase of viscosity with conversion and the corresponding high decrease of the phase separation rate.

(e) The concentration of dispersed phase particles, P, decreases with temperature due to the decrease in the phase separation rate with respect to the polymerization rate ($E_D < E$).

(f) The range of compositions of both phases agrees with the one experimentally found. The high volume fraction of epoxy–amine copolymer in dispersed domains is explained by the shape of the Flory–Huggins equation. The compositions demixed at the beginning of phase separation (accounting for most of V_D) contain a large volume fraction of epoxy–amine copolymer. The trend for ϕ_R^C vs. ϕ_{Ro} is, however, inverse to the one experimentally reported.

(g) Phase separation inside dispersed domains has to take place because their overall composition is located in the unstable region of the phase diagram.

(h) The range of particle sizes is in rough agreement with model predictions.

Therefore, a nucleation-growth mechanism gives a reasonable explanation of most of the experimental trends for this particular system. This gives an indirect confirmation of the very low values of interfacial tensions playing a role during the phase separation process.

A frame for the explanation of the phase separation process in rubber-modified epoxies has been developed. Further work may be related to the improvement of the thermodynamic and kinetic basis by removing some of the hypotheses carried out in the analysis, or to the extension to formulations using different rubbers than butadiene–acrylonitrile copolymers, like polysiloxanes or polyacrylates,[24–27] or to the use of engineering thermoplastics like PES or PEI in epoxy formulations.[28–32] In this last case, new situations, like the vitrification curve of the epoxy copolymer–engineering thermoplastic, have to be considered in the analysis, because phase separation may be constrained by vitrification, depending on the location of the predicted composition for the dispersed phase and the T_g vs. composition curve. Of great interest will be also to follow the evolution of morphology at the early stages of phase separation. This would give a direct evidence of the phase separation mechanism.

This work was performed in the frame of a cooperation program between the National Research Councils of France (CNRS) and Argentina (CONICET). The financial support of both institutions is gratefully acknowledged.

REFERENCES

1. D. Verchère, H. Sautereau, J. P. Pascault, S. M. Moschiar, C. C. Riccardi, and R. J. J. Williams, *J. Appl. Polym. Sci.*, **41**, 467 (1990).
2. D. Verchère, J. P. Pascault, H. Sautereau, S. M. Moschiar, C. C. Riccardi, and R. J. J. Williams, *J. Appl. Polym. Sci.*, **41**, 701 (1991).
3. R. J. J. Williams, J. Borrajo, H. E. Adabbo, and A. J. Rojas, in *Rubber-Modified Thermoset Resins*, Adv. Chem. Ser. No. 208, C. K. Riew and J. K. Gillham, Eds., American Chemical Society, Washington DC, 1984, p. 195.
4. A. Vazquez, A. J. Rojas, H. E. Adabbo, J. Borrajo, and R. J. J. Williams, *Polymer*, **28**, 1156 (1987).
5. D. Verchère, H. Sautereau, J. P. Pascault, C. C. Riccardi, S. M. Moschiar, and R. J. J. Williams, *Macromolecules*, **23**, 725 (1990).
6. G. F. Roginskaya, V. P. Volkov, L. M. Bogdanova, A. Y. Chalykh, and B. A. Rosenberg, *Polym. Sci. USSR*, **25**, 2305 (1983).
7. L. T. Manzione, J. K. Gillham, and C. A. McPherson, *J. Appl. Polym. Sci.*, **26**, 889 (1981).
8. L. T. Manzione, J. K. Gillham, and C. A. McPherson, *J. Appl. Polym. Sci.*, **26**, 907 (1981).

9. S. Montarnal, J. P. Pascault, and H. Sautereau, in *Rubber-Toughened Plastics,* Adv. Chem. Ser. No. 222, C. K. Riew, Ed., American Chemical Society, Washington DC, 1989, p. 193.
10. H. S. Y. Hsich, *Proc. 34th Int. SAMPE Symp.,* 1989, p. 884.
11. K. Yamanaka, Y. Takagi, and T. Inoue, *Polymer,* **60,** 1839 (1989).
12. D. Verchère, H. Sautereau, J. P. Pascault, S. M. Moschiar, C. C. Riccardi, and R. J. J. Williams, *Polymer,* **30,** 107 (1989).
13. J. Borrajo, C. C. Riccardi, S. M. Moschiar, and R. J. J. Williams, in *Rubber-Toughened Plastics,* Adv. Chem. Ser. No. 222, C. K. Riew, Ed., American Chemical Society, Washington DC, 1989, p. 319.
14. J. E. Sohn, J. A. Emerson, P. A. Thompson, and J. T. Koberstein, *J. Appl. Polym. Sci.,* **37,** 2627 (1989).
15. J. Noolandi and K. M. Hong, *Macromolecules,* **17,** 1531 (1984).
16. S. H. Anastasiadis, I. Gancarz, and J. T. Koberstein, *Macromolecules,* **22,** 1449 (1989).
17. D. Chen, J. P. Pascault, and D. Sage, *Makromol. Chem.,* to appear.
18. G. Langhammer and L. Nester, *Makromol. Chem.,* **88,** 179 (1965).
19. G. Riess, in *Initiation à la Chimie et à la Physicochimie Macromoléculaires, Vol. 6, Mélanges des Polymères,* G.F.P., Strasbourg, 1986, p. 73.
20. R. H. Doremus, *Rates of Phase Transformations,* Academic, Orlando, FL, 1985, p. 65.
21. T. K. Sherwood, R. L. Pigford, and C. R. Wilke, *Mass Transfer,* McGraw-Hill, New York, 1975.
22. G. L. Gaines, Jr., *Polym. Eng. Sci.,* **12,** 1 (1972).
23. E. Butta, G. Levita, A. Marchetti, and A. Lazzeri, *Polym. Eng. Sci.,* **26,** 63 (1986).
24. J. S. Rifle, I. Yilgor, C. Tran, G. L. Wilkes, J. E. McGrath, and A. K. Banthia, in *Epoxy Resin Chemistry II,* Symp. Ser. No. 221, R. S. Bauer, Ed., American Chemical Society, Washington DC, 1983, p. 21.
25. E. M. Yorkgitis, C. Tran, N. S. Eiss, Jr., T. Y. Hu, I. Yilgor, G. L. Wilkes, and J. E. McGrath, in *Rubber-Modified Thermoset Resins,* Adv. Chem. Ser. No. 208, C. K. Riew and J. K. Gillham, Eds., American Chemical Society, Washington DC, 1984, p. 137.
26. T. Takahashi, N. Nakajima, and N. Saito, in *Rubber-Toughened Plastics,* Adv. Chem. Ser. No. 222, C. K. Riew, Ed., American Chemical Society, Washington DC, 1989, p. 243.
27. A. K. Banthia, P. N. Chaturvedi, V. Jha, and V. N. S. Pendyala, in *Rubber-Toughened Plastics,* Adv. Chem. Ser. No. 222, C. K. Riew, Ed., American Chemical Society, Washington DC, 1989, p. 343.
28. J. L. Hedrick, I. Yilgor, G. L. Wilkes, and J. E. McGrath, *Polym. Bull.,* **13,** 201 (1985).
29. C. B. Bucknall and I. K. Partridge, *Polym. Eng. Sci.,* **26,** 54 (1986).
30. R. S. Raghava, *J. Polym. Sci. Polym. Phys. Ed.,* **25,** 1017 (1987).
31. R. S. Raghava, *J. Polym. Sci. Polym. Phys. Ed.,* **26,** 65 (1988).
32. C. B. Bucknall and A. H. Gilbert, *Polymer,* **30,** 213 (1989).

Received December 14, 1989
Accepted March 13, 1990